Korea Polymer Journal, Vol. 9, No. 4, pp 185-196 (2001)

Korea Polymer Journal

Volume 9, Number 4 August 31, 2001

Feature Article

Self-Assembly of Triblock Copolymers in Melts and Solutions

Seung Hyun Kim and Won Ho Jo*

Hyperstructured Organic Materials Research Center, and School of Materials Science and Engineering, Seoul National University, Seoul 151-742, Korea

Received June 16, 2001

Abstract : The self-assembly of block copolymers can lead to a variety of ordered structures on a nanometer scale. In this article, the self-assembling behaviors of triblock copolymers in the melt and the selective solvent are described with the results obtained from the computer simulations. With the advances of computing power, computer simulations using molecular dynamics and Monte Carlo techniques make it possible to study very complicated phenomena observed in the self-assembly of triblock copolymer. Taking full advantage of the computer simulation based on well-defined model, the effects of various structural and thermodynamic parameters such as the copolymer composition, the block sequence, the pairwise interaction energies, and temperature on the self-assembly are discussed in some detail. Some simulation results are compared with experimental ones and analyzed by comparing them with the theoretical treatment.

Introduction

Block copolymers, composed of two or more chemically distinct repeating units, have attracted considerable attention during the past two decades because of their applications in a wide range of fields from material science to biology.[1-3] The key feature of block copolymers that has fascinated scientists and engineers is their ability to spontaneously self-assemble in the melt or solution into a variety of ordered structures with nanoscale periodicities. Furthermore, the self-assembly of block copolymers, depending upon the molecular architecture and thermodynamic conditions, yields an extraordinarily rich and complex phase diagram, which enables them to have a variety of properties tunable to many applications and to serve as a good model system for the study of self-assembly.

In the melt, ABA-type triblock copolymers exhibit very similar self-assembly behavior to AB diblock copolymers. In addition to the lamellar, cylindrical and spherical morphologies, more complex phases,

*e-mail : whjpoly@plaza.snu.ac.kr

such as the bicontinuous gyroid and perforated layer structures have been identified for the block copolymers, depending on the composition, the degree of polymerization, and thermodynamic interaction.[2] ABC triblock copolymers are expected to show even more complex phase behaviors due to the increased number of independent compositions and thermodynamic interaction parameters. Indeed, some of complex morphologies have recently been identified by several research groups.[4-11] However, there are still so wide areas in the parameter space that have not been exploited because of strongly coupled relationship between a number of structural and thermodynamic parameters.

In a solvent which is selective for one of their constituents, ABA-type triblock copolymer can self-assemble into micelles.[1,2] In general, the micelle consists of two phases, an inner core predominantly composed of insoluble blocks and an outer corona composed of the soluble blocks and the solvent molecules. However, ABA triblock copolymers exhibit quite different self-association behavior from AB diblock copolymers depending on the solvent selectivity. In other words, ABA triblock copolymers in a selective solvent for the middle block B behave differently from those in a selective solvent for the end blocks A. A number of efforts have been made to clarify the self-association of the triblock copolymer in a selective solvent,[12-20] but there have been few studies for a direct comparison of the micelle formation and structural characteristics between two different triblock copolymer systems (viz., ABA and BAB triblock copolymers in a selective solvent for A blocks).

Therefore, in this article, we focus on the self-assembly of ABC triblock copolymers in the melt and of ABA- and BAB-type triblock copolymers in a selective solvent for block A, based on the results from computer simulations performed in our laboratory.[21-25] Computer simulation may provide a powerful tool to solve these complicated problems since it is based on well-defined model and all degrees of freedom are known explicitly. Since we are concerned with the mesoscale behavior of triblock copolymers, the simplified coarse-grained model that can effectively represent the general features of copolymer chains is used for the simulation. In the following, the simulation model and methods for studying the self-assembly of block copolymers in the melt and solution will be presented and their representative results will be discussed in detail.

Triblock Copolymer in Melt

Model and Simulation Method. Most of the previous simulation studies on the self-assembly of block copolymers were carried out by using the lattice Monte Carlo (MC) method, which is computationally convenient and fast.[26-29] However, this lattice model has some serious problems for the simulation of self-assembling systems. The most important problem is that the periodicity of microphase separated structures must match with the dimension of the simulation box in order to obtain successful results, since the box dimension is fixed throughout simulation in lattice model. In other words, when the periodicity of phase separated structures dose not match with the dimension of simulation box, the structures may deviate from their preferred shapes in order to be commensurate with the periodic images due to the boundary conditions, leading to a distorted structure of ordered phases. To overcome this problem, the isothermal-isobaric molecular dynamics (MD) simulations based on the continuum model are here adopted. Accordingly, the volume and shape of simulation box are allowed to fluctuate according to the periodicity of ordered phases while the pressure, the temperature and the number of chain molecules are fixed.

The coarse-grained continuum model used for the simulation of ABC triblock copolymer is of bead-spring type.[30,31] In this model, each chain consists of N beads with the identical size. The total chain length is set constant $N = 80$ for all cases simulated. Symmetric triblock copolymers, in which both end blocks have equal chain lengths, are only considered. Therefore, the volume fractions (f_A and f_C) of blocks A and C are given by the volume fraction (f_B) of middle block B as $f_A = f_C = (1-f_B)/2$. Each bead interacts with only two types of potential, E_{vdw} and E_l. E_{vdw} is a Lennard-Jones (LJ) potential acting between any pair of seg-

ments as given by

$$E_{vdw} = 4\varepsilon_{ij}\left[\left(\frac{\sigma_{ij}}{r}\right)^{12} - \left(\frac{\sigma_{ij}}{r}\right)^{6} - \left(\frac{\sigma_{ij}}{r_c}\right)^{12} + \left(\frac{\sigma_{ij}}{r_c}\right)^{6}\right] \quad r \le r_c \tag{1}$$

where r is the distance between the ith and jth segment and r_c is the cut-off distance set as $r_c = 2^{1/6}\sigma$ to make the potential purely repulsive. ε_{ij} and σ_{ij} are the LJ energy and length parameters for segments i and j, respectively. The length parameters are chosen as $\sigma_{AA}=\sigma_{BB}=\sigma_{CC}=\sigma_{AB}=\sigma_{BC}=\sigma$ so that all types of segments have the same interaction range and the same molar volume. The energy parameters are set as $\varepsilon_{AA}=\varepsilon_{BB}=\varepsilon_{CC}=\varepsilon$, $\varepsilon_{AB}/\varepsilon=5$, $\varepsilon_{BC}/\varepsilon=10$, and $\varepsilon_{CA}/\varepsilon=2$ (i.e., $\varepsilon_{AC} < \varepsilon_{AB} < \varepsilon_{BC}$). The reason why we choose the interaction energies as such is for comparison with experimental results for PS-PB-PMMA triblock copolymers reported by Stadler *et al.*,[6-10] where $\chi_{PS\text{-}PMMA} < \chi_{PS\text{-}PB} < \chi_{PB\text{-}PMMA}$. E_l is bond stretching potential along the chains, as given by

$$E_l = \frac{1}{2}k_b(l - l_0)^2 \tag{2}$$

where k_b is the energy parameter of the potential, l is the distance between two neighboring segments of the same chain, and l_0 is a length parameter at which the potential has a minimum value. We have chosen $k_b = 10^3\varepsilon/\sigma^2$ and $l_0 = 0.75\sigma$ to avoid the bond crossing.[32]

The initial configurations are randomly generated in a cubic simulation box and then energy-minimized. Before implementing the isothermal-isobaric dynamics, the systems are fully relaxed by the canonical ensemble (NVT) molecular dynamics. The initial number density of triblock copolymer is set as $\rho = 0.85\sigma^{-3}$, and the temperature is set as $T = \varepsilon/k_B = 1.0$ where k_B is the Boltzmann constant. The pressure obtained from NVT simulation is used as an external pressure in the following isothermal-isobaric simulation.

Composition Effects. Figure 1 shows the simulation results for $A_{27}B_{26}C_{27}$ triblock copolymer with $f_A = f_B = f_C = 0.33$, where the number in subscript indicates the chain length of each block. The snapshot in Figure 1(a) clearly displays the lamellar morphology. This lamellar structure is

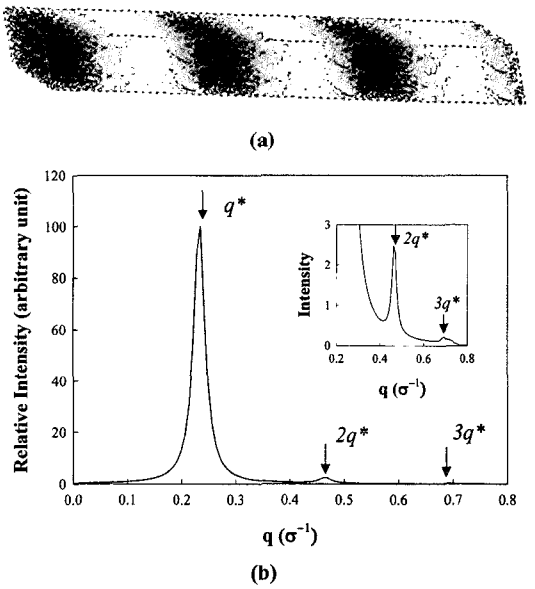

Figure 1. (a) Snapshot of $A_{27}B_{26}C_{27}$, where A, B and C segments are colored black, gray and white, respectively. Simulated scattering pattern of $A_{27}B_{26}C_{27}$ from snapshot (a) is shown in (b) where the intensity of peaks is normalized with respect to that of the first order peak.

supported by the calculated scattering pattern in Figure 1(b), where characteristic Bragg-peaks of higher order are observed at the integer multiples of the scattering vector of the first maximum (q^*). As shown in Figure 1(a), A and C lamellae (black and white, respectively) are almost two times as thick as B lamellae (gray), since triblock copolymers in the lamellar structure are laid sequentially in a way of ABC and CBA. Our result agrees well with experimental one reported by Stadler *et al.*[6,7] under similar thermodynamic conditions.

Change of midblock length at a fixed total chain length and thus of composition of ABC copolymer will result in the change of the lamellar thickness and eventual morphology transition. The snapshot of triblock copolymer $A_{32}B_{16}C_{32}$ with $f_B = 0.2$ shows that the ordered structure seems to be a lamellar-type morphology, as can be seen in Figure 2(a). However, due to shorter chain length of midblock B, the microdomain of block B becomes cylinders in shape and as a result, A/C interfaces are formed despite the absence of A-C junction in the triblock copolymer. Their schematic representation corresponding to the simulated morphol-

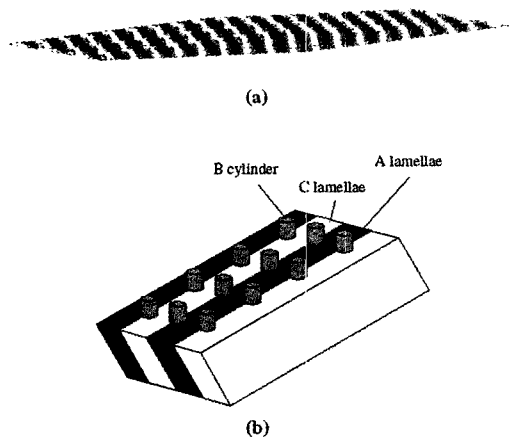

Figure 2. (a) Snapshot of $A_{32}B_{16}C_{32}$, where A, B and C segments are colored black, gray and white, respectively. Schematic representation of the morphological structure for $A_{32}B_{16}C_{32}$ is shown in (b), where B cylinders at the interface between A and C lamellae in $A_{32}B_{16}C_{32}$ are developed.

ogy from $A_{32}B_{16}C_{32}$ triblock is shown in Figure 2(b). For $A_{35}B_{10}C_{35}$ triblock with much smaller f_B, the microdomains of block B show more discrete feature at the interface between A and C lamellae, as shown in Figure 3(a). That is, the cylinders formed at the A/C interface for $A_{32}B_{16}C_{32}$ break down into the isolated domains for $A_{35}B_{10}C_{35}$. It can also be seen that some residues of block B are included in A lamellae due to relatively less unfavorable interaction of block B with block A than with block C.

ABC triblock copolymers with the midblock B as a major component exhibit totally different structure. Figure 4 shows the simulation results for $A_{20}B_{40}C_{20}$ copolymer with $f_B = 0.5$. The snapshot in Figure 4(a) shows a very peculiar and complicated structure, and the domains of the minority components appear to be connected with each other. This morphology is very similar to the gyroid structure which has been predicted by the theoretical approach of Masten[33] and Phan and Fredrickson.[34] The simulation result for $A_{10}B_{60}C_{10}$ with larger volume fraction of midblock B (f_B = 0.75) is shown in Figure 5. In this case, two end blocks form one spherical domain in the matrix composed of midblock B due to relatively less incompatibility between the blocks A and C, as

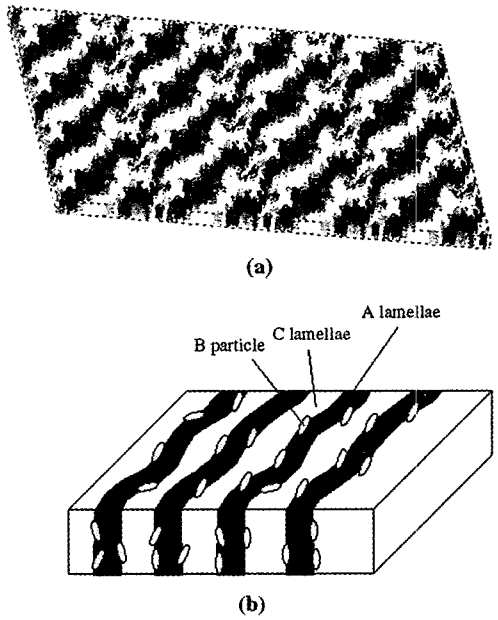

Figure 3. (a) Snapshot of $A_{35}B_{10}C_{35}$, where A, B and C segments are colored black, gray and white, respectively. Schematic representation of the copolymer morphology is shown in (b), where B particles between A and C lamellae in $A_{35}B_{10}C_{35}$ are observed.

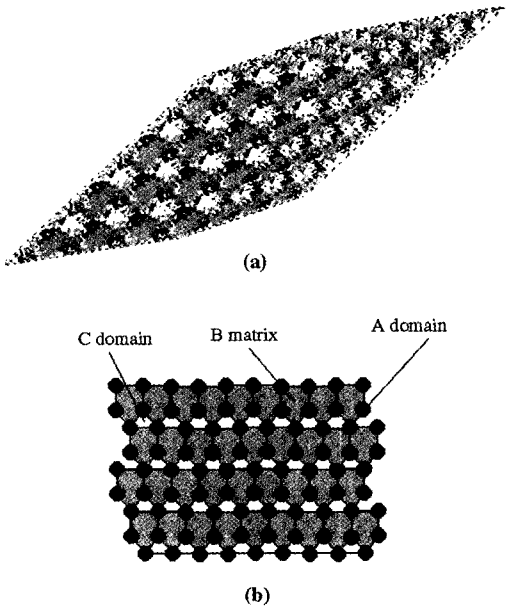

Figure 4. (a) Snapshot of $A_{20}B_{40}C_{20}$, where A, B and C segments are colored black, gray and white, respectively. Schematic representation of tricontinuous structure of $A_{20}B_{40}C_{20}$ is shown in (b).

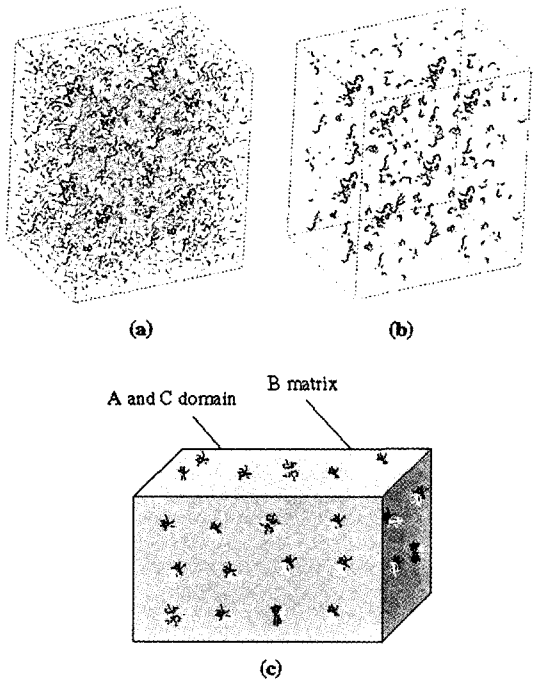

Figure 5. (a) Snapshot of $A_{10}B_{60}C_{10}$, where A, B and C segments are colored black, gray and white, respectively. For clarity, the B segments of matrix are removed from snapshot (a) in (b). Schematic representation of micelle-type structure of $A_{10}B_{60}C_{10}$ is shown in (c).

schematically shown in Figure 5(c).

Sequence Effects. It is expected that the sequence of three blocks (i.e., A-B-C, B-C-A, or C-A-B) plays an important role in the self-assembly of ABC triblock copolymer since it affects the thermodynamic conditions between midblock and endblocks. Figure 6 shows the sequence effects of $A_{32}B_{16}C_{32}$ triblock copolymers. Unlike the morphology of $A_{32}B_{16}C_{32}$ (Figure 2), the snapshot of $B_{16}C_{32}A_{32}$ (Figure 6(a)) shows that a cylindrical core-shell morphology in which a B cylinder is surrounded by a C cylindrical shell is formed in the A matrix. This morphology is similar to the "cylinder in cylinder" morphology as previously reported for PS-PB-PMMA triblock copolymer.[10] Considering the relative magnitude of interactions and block connectivity, this result can be explained as follows. Since the incompatibility between B and C is larger than that between C and A, the system tends to reduce the interfacial area between B and C, as compared to that between C and A. The formation of interface between B and C is unavoidable due to the connectivity between the blocks B and C. As a consequence, the block C may form the shell around the core cylinder of block B with smaller volume fraction. The morphology developed from $C_{32}A_{32}B_{16}$ triblock exhibits a different structure from the $A_{32}B_{16}C_{32}$ and $B_{16}C_{32}A_{32}$ triblocks, as shown in Figure 6(b). The overall morphology of $C_{32}A_{32}B_{16}$ is lamellar, but the block B forms cylinders in shape

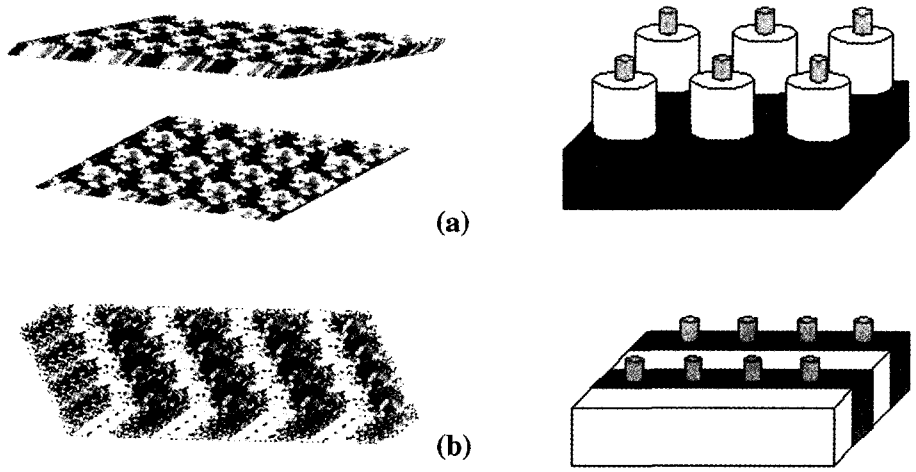

Figure 6. Snapshot of triblock copolymers with $f_A = f_C = 0.4$ and $f_B = 0.2$: (a) $B_{16}C_{32}A_{32}$; (b) $C_{32}A_{32}B_{16}$, where A, B and C segments are colored black, gray and white, respectively. Schematic representations of each morphological structure are shown in the right side.

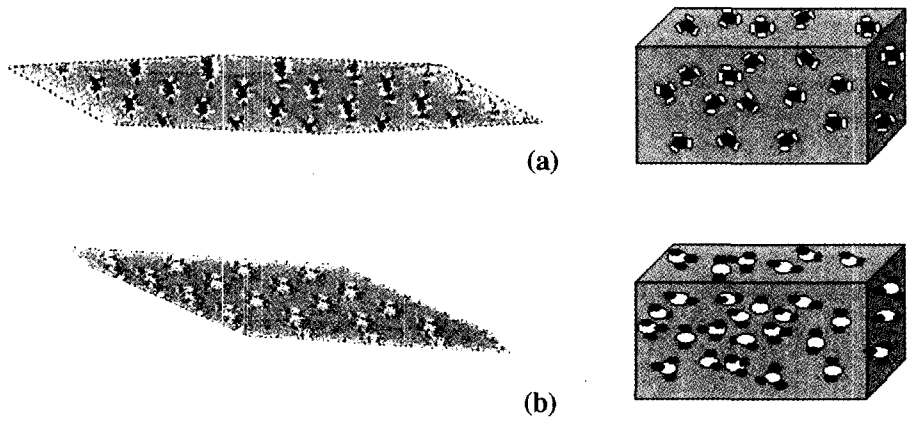

Figure 7. Snapshot of triblock copolymers with $f_A = f_C = 0.125$ and $f_B = 0.75$: (a) $B_{60}C_{10}A_{10}$; (b) $C_{10}A_{10}B_{60}$, where A, B and C segments are colored black, gray and white, respectively. Schematic representations of each morphological structure are shown in the right side.

due to the shorter chain length of endblock B. As mentioned above, the interaction between B and C is more repulsive than that between A and B, and therefore this may suppress the direct contact between B and C components, leading to the inclusion of B cylinder into A lamellar microdomain. Here, it is noted that the block B is not directly connected to the block C contrary to the case of $B_{16}C_{32}A_{32}$ triblock.

The sequence effect of $A_{10}B_{60}C_{10}$ with spherical morphology in the matrix of midblock B is observed in Figure 7. When the block sequence is changed to B-C-A ($B_{60}A_{10}C_{10}$), the blocks A and C seem to form one spherical domain in the B matrix (see Figure 7(a)), as in the case of A-B-C. However, the midblock C is located at the phase boundary between spheres and matrix because the midblock C is connected with both end blocks. This explanation is also applicable to the C-A-B ($C_{10}A_{10}B_{60}$) case, where the block A is located at the interface between the matrix B and the dispersed phase C, as shown in Figure 7(b).

Triblock Copolymers in a Selective Solvent

Model and Simulation Method. Several simulation studies on the self-assembly (i.e., micellization) of block copolymers in a selective solvent have been reported.[13,35-37] Most of them are based on the canonical ensemble. From those studies, it was revealed that the simulation box should be large enough not to be affected by finite size effects. Since the system must contain a large number of micelles at the critical micelle concentration (cmc) for reliable results, very long simulations are also required to equilibrate the micellar size distribution. To overcome these limitations, the grand-canonical Monte Carlo (GCMC) simulation method is used to investigate the micellization of ABA and BAB triblock copolymers. This GCMC technique has several advantages in studying the micellization behavior of amphiphilic molecules over the simulations based on the canonical ensemble, such as the use of smaller simulation box, faster equilibration of micellar size distribution, and so on.[38,39]

All simulations for the micellization of ABA and BAB are performed on a cubic lattice in the grand canonical ensemble. In this case, the chemical potential, volume and temperature of the system are fixed while the density of the system is allowed to fluctuate throughout simulation. ABA and BAB symmetric triblock copolymers are represented as a chain of connected segments on a lattice with the coordination number of 26. All unoccupied sites on the lattice are considered as a solvent. The interaction ε_{BB} between B-B segments is set to be 1, and all the other pairwise interactions are set to be zero. As a result, the simulation model represents a solution of ABA or BAB in a solvent selective for block A. The total chain length and

composition of triblock copolymer are kept constant as $N = 30$ and $f_B = 0.33$, respectively, for both ABA and BAB. The chain configurations are sampled by means of mixed moves of 50% reptation moves and 50% chain insertion/deletion steps. To improve the efficiency of the GCMC simulation for chain molecules, the configurational bias Monte Carlo (CBMC) method is applied in the general manner.[39] The linear dimension of simulation box is $L = 40$.

Basic Micellar Parameters. In GCMC simulations, the chemical potential and the temperature of triblock copolymer systems are given as input parameters, and their average volume fraction will be obtained through the simulation. Figure 8 shows typical data for the distribution of association number for both ABA and BAB copolymers at different average volume fractions, where the temperature is $T = 4.5$. Both triblock copolymers clearly exhibit a bimodal distribution of the association number at volume fractions above some critical one, which is a good evidence for the formation of thermodynamically stable micelle. However, there is a large difference in the critical concentration at which the system shows the bimodal distribution between the two copolymers, in spite of the same chain length and composition. Judging from the distribution curve, the ability to self-assemble into micelles is considerably reduced for BAB copolymers as compared to ABA. This behavior can be ascribed to the additional entropy loss of BAB chains due to the looping geometry of the middle block because both end blocks should stay in the same micellar core to form micelles. It can be seen that the micelles of BAB are much larger in size and much broader in its distribution than ABA. All these results can be observed at all other temperatures simulated.

For direct comparison of the micellar size of ABA and BAB systems, the mean micellar size is calculated and its results are presented in Figure 9. The mean micellar size is defined as the weight-averaged association number M_w obtained from the association number distribution. Figure 9 clearly shows that BAB copolymer forms the micelles of much larger size than ABA. It can also be seen that the mean micellar size depends on the temperature, especially for ABA copolymers.

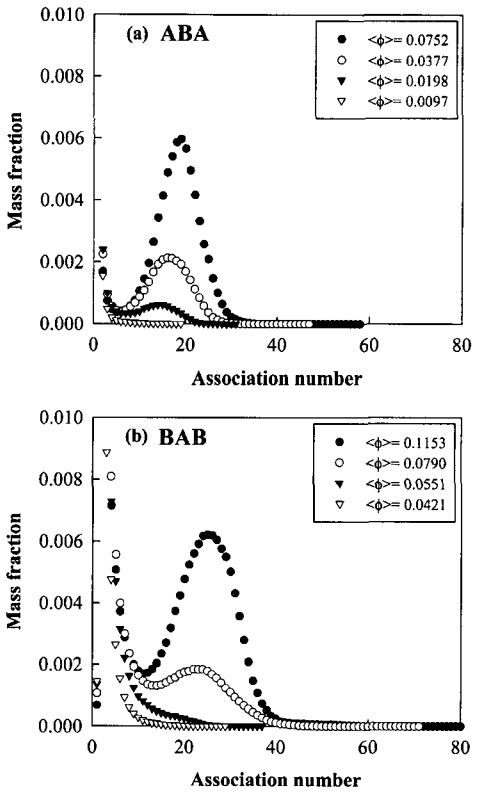

Figure 8. Mass fraction of micelles as a function of the association number when ABA (a) and BAB (b) block copolymers are micellized at various average volume fraction of copolymers at $T = 4.5$.

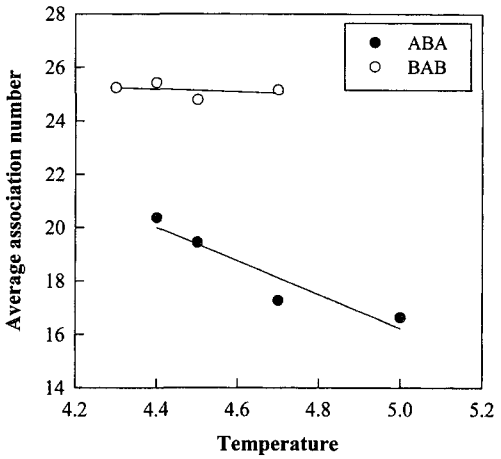

Figure 9. Change of the mean micellar size with temperature for ABA and BAB systems.

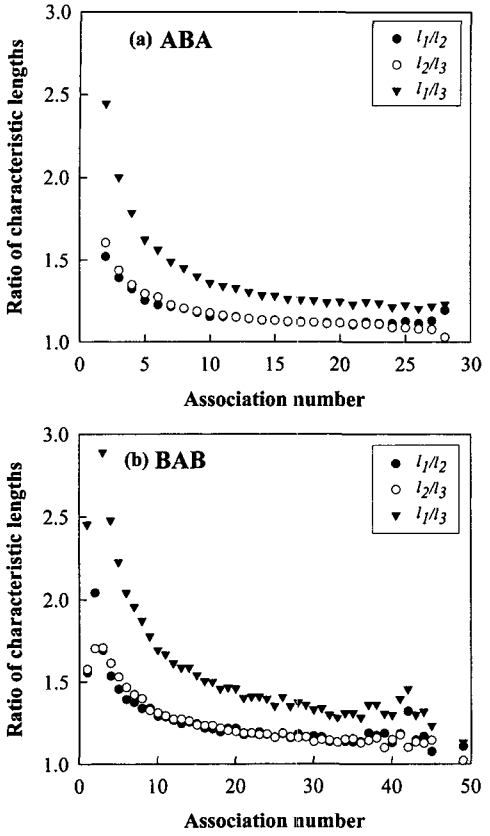

Figure 10. Ratio of characteristic lengths as a function of the association number for (a) ABA and (b) BAB copolymers at T = 4.5.

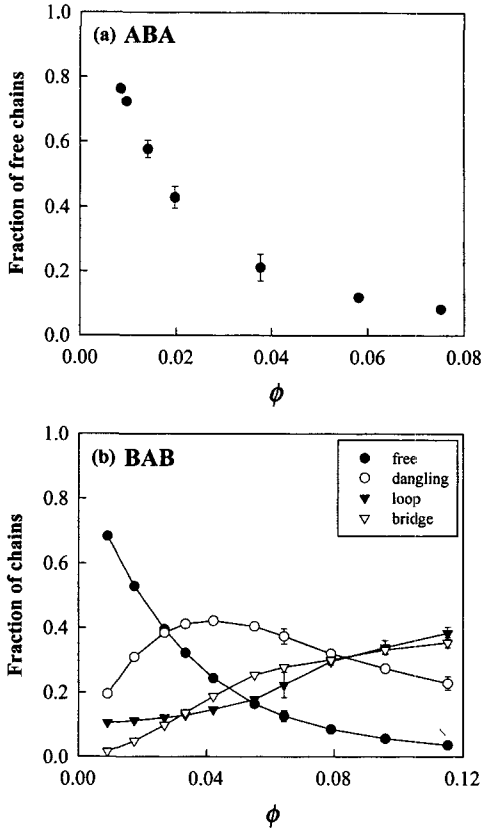

Figure 11. Change of the fraction of each conformation with the average volume fraction for (a) ABA and (b) BAB copolymers at T = 4.5.

The shape of micelle can be quantitatively characterized by analyzing the principal moments of inertia of micelle. The set of eigenvalues (λ_1, λ_2, and λ_3;$\lambda_1>\lambda_2>\lambda_3$) of the moment of inertia matrix is evaluated, and a characteristic length is determined to be $l_i = \lambda_i^{1/2}$ for i = 1, 2, 3. A measure of the micellar asphericity, which is dependent on the micellar size, can be obtained by measuring l_1/l_2, l_2/l_3, and l_1/l_3. For a spherical micelle, $l_1/l_2 = l_2/l_3 = l_1/l_3 = 1$, and for a cylindrical one, $l_1/l_3>>1$, $l_2/l_3 = 1$. When the ratios of characteristic lengths are plotted against the association number, it is observed that the characteristic length ratios are less than 2 for most of micelles except the small aggregates and becomes constant at large association number, as shown in Figure 10, indicating that the micelles formed by both types of triblock copolymers are nearly spherical.

Due to higher entropic penalty of BAB copolymers in the micelle, some of them exist as the so-called dangling chain that has one end in the core and the other in the solution, which was confirmed in the snapshot of individual micelles (not shown here). As the copolymer concentration increases in the solution, these free end blocks of dangling chains can participate in the core of another micelle or self-assemble into new micelles, resulting the branched or network structure with bridge chain. Therefore, it is informative to analyze the status of copolymer chains as a function of concentration. For ABA, the copolymer exists either in a micelle or in a solution. As shown in Figure 11(a), the fraction of free chains decreases with increasing the copolymer concentration. For BAB, the copolymer chain exists as one of four states, namely, free, dangling, loop, and bridge chain. As

shown in Figure 11(b), the fraction of free chain rapidly decreases with the concentration, as in the case of ABA. At low concentration, the fraction of dangling chain is larger than those of the loop and bridge chains. This is because the copolymer chains are not able to form a thermodynamically stable micelle but form small aggregates below the cmc. As the concentration increases, the fraction of dangling chains shows a maximum around the cmc and then decreases, implying the formation of the typical micelles. The fractions of loop and bridge chains steadily increase as the concentration increases, since they contribute significantly to the formation of the micelles.

Thermodynamic Analysis. In order to analyze the micellization behavior of the two different triblock copolymers, the multiple equilibrium model, in which the micelles of different sizes are in equilibrium with each other, is used. According to this model, the micellar size distribution can be obtained as below:[40,41]

$$x_M = M\frac{(a_1 x_1)}{a_M}\exp\left[-M\frac{(\mu_M^0 - \mu_1^0)}{k_B T}\right] \quad (3)$$

where x_M is the mole fraction of chains present in micelles with association number M, μ_i^0 the chemical potential per molecule in a micelle of size i in a dilute reference state, and a_i an activity coefficient. The activity coefficient can be estimated from the second virial coefficient between two micelles following the approach proposed by von Gottberg *et al.*[42] At low concentrations, the micelle-micelle interaction may be ignored and thus the excess chemical potential per molecule can be given as[40]

$$\frac{(\mu_M^0 - \mu_1^0)}{k_B T} = \frac{1}{k_B T}\left(\frac{\bar{U}^M}{M} - \bar{U}^1\right) - \frac{1}{k_B}\left(\frac{S^M}{M} - S^1\right) \quad (4)$$

The excess chemical potential per molecule (μ_M^0-μ_1^0) can be calculated from the micellar size distribution using eq. (3). The potential energy $\bar{U}^M$ for a micelle of size M is also calculated during the simulation, and therefore the excess enthalpy per molecule, $[(\bar{U}^M/M) - \bar{U}^1]/k_B T$, can be estimated directly from the simulation. The last term $[(S^M/M) - S^1]/k_B$ is the excess entropy per molecule, and the entropic terms related to the translation of the micelles cancel out in eq. (4). Therefore, S^M is regarded as the entropy associated with packing the chains into the micelle. Figure 12 compares the excess thermodynamic properties of ABA with those of BAB under the same condition of micellization. The excess chemical potential of ABA is slightly lower than BAB, indicating that the micellization of ABA copolymers is more favorable. This is attributed to the loose or open micellar structure of BAB by the presence of dangling and bridge chains, which leads to much lower excess enthalpy and thus lower excess chemical potential than that of ABA. Such imperfect structure of micelles of BAB copolymers, however, gives much lower packing entropy of their micelles than those of ABA, as shown in Figure 12. As the micellar size increases, this packing entropy of chains in micelles decreases and eventually limits further growth in the micelle size due to an increased self-crowding at the micellar surface. Therefore, BAB copolymers with a smaller decrease in the excess entropy per molecule may form the micelles with larger size than ABA.

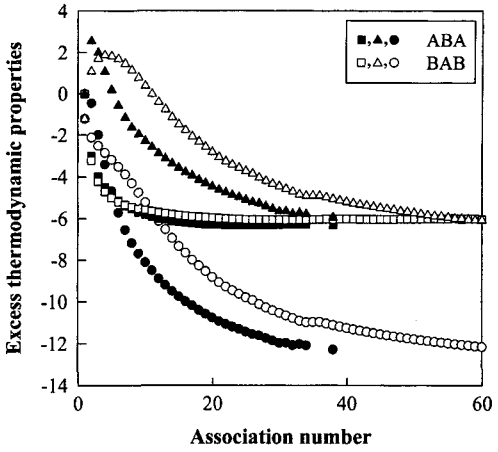

Figure 12. The excess enthalpy (●, ○), the excess chemical potential, (■,□), and the excess entropy (▲, △) per copolymer chain as a function of the micellar size. The filled and open symbols correspond to ABA and BAB system, respectively.

The critical micelle concentration (cmc) is generally defined as the concentration at which micelles first appear in solution at a given temeperature. By the closed association mechanism through the mass-action model, the standard free energy of micelle formation, i.e., the standard free energy

change for the transfer of 1 mol of copolymer chain from solution to micellar phase, is related to the cmc as follows:

$$\Delta G^0 = RT\ln x_{cmc} \quad (5)$$

where x_{cmc} is the cmc in mole fraction unit. The standard molar enthalpy of micelle formation is then given as below by applying the Gibbs-Helmholtz equation:

$$\Delta H^0 = R[d\ln x_{cmc}/d(1/T)] \quad (6)$$

If one assumes that ΔH^0 is approximately constant within a certain temperature range, eq. (6) can be integrated to yield

$$\ln x_{cmc} = \Delta H^0/RT + \text{constant} \quad (7)$$

In the simulation, the cmc is obtained by calculating the osmotic pressure from the GCMC simulation combined with the multiple histogram method.[43] By using the histogram method,[44,45] several simulation results are collected to estimate the grand canonical partition function, from which the osmotic pressure can directly be calculated. The related equations and procedure can be found elsewhere.[24] According to eq. (7), the cmc for both types of block copolymers is plotted on a logarithmic scale against the inverse temperature in Figure 13. The multiple histogram method can predict the cmc values at temperatures where the simulation has not been carried out. It is clear that all cmc values, except for those of BAB at high temperature, are well fitted by a straight line, irrespective of block sequence of triblock copolymers, which implies that the two types of triblocks form micelles according to the closed association mechanism. As expected, BAB has higher cmc values than ABA. From the slope of straight lines in Figure 13, the standard enthalpies of micellization are evaluated, as can be realized from eq. (7), yielding ΔH^0 = -60.3 kJ/mol for ABA and ΔH^0 = -54.4 kJ/mol for BAB, respectively. The negative value of ΔH^0 implies that the micellization is an enthalpy-driven process. As discussed above, the loose and imperfect structure of BAB micelles by the dangling and bridge chains lead to less negative value of ΔH^0 for BAB than ABA.

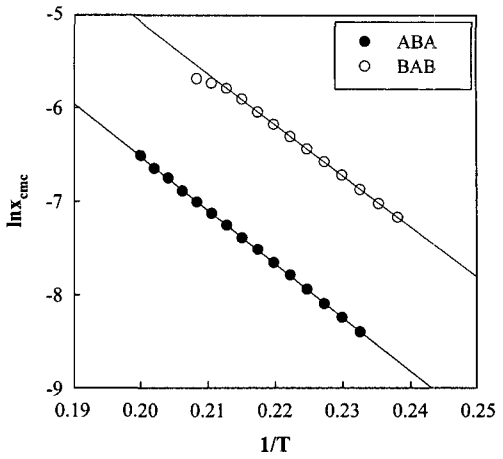

Figure 13. Plots of the critical micelle concentration *versus* the reciprocal temperature for ABA and BAB copolymer systems on semi-logarithmic scale.

Summary

In this article, we described the self-assembly behaviors of ABC-type and ABA-type triblock copolymers in the melt and the solution, respectively, with the simulation results obtained through various simulation models and methods.

Symmetric ABC triblock copolymers in the melt produced a variety of ordered structures, depending on the copolymer composition, the block sequence and the relative interactions. When the midblock B is a minor component, the structure of block B is changed from lamellar, cylindrical to spherical morphology at the interface between A/C lamellae as the volume fraction of block B decreases. When the midblock B is a major component, the morphologies are changed from tricontinuous to spherical structures in the matrix composed of midblock as the volume fraction of block B increase. It was also found that block sequence (A-B-C, B-C-A, or C-A-B) strongly affects the morphology of triblock copolymer.

ABA and BAB triblock copolymers exhibited very different self-assembling behaviors in a solvent selective for block A. BAB triblock copolymers have a reduced ability to self-assemble into micelles, yielding higher cmc values than ABA. This difference arises from an additional entropic

penalty associated with looping conformation of the midblock of BAB copolymers. Nevertheless, BAB copolymers formed the micelles with larger size and broader size distribution than ABA since BAB copolymers have much lower entropy change associated with packing of chains in the micelle due to the loose micellar structure.

With the remarkable development of computing power and algorithm, computer simulation has become an established method of research in polymer science and a useful tool in attacking very complicated problems, complementing both experiment and theory. As discussed above, our computer simulation can effectively provide an understanding for the basic principles of self-assembly of block copolymers and a guideline for designing new mircophase morphology by tailoring block copolymers.

Acknowledgement. The authors thank the Korea Science and Engineering Foundation (KOSEF) for its financial support through the Hyperstructured Organic Materials Research Center.

References

(1) S. E. Webber, P. Munk, and Z. Tuzar, *Solvents and Self-Organization of Polymers,* Kluwer Academic Publishers, Dordrecht, 1996.
(2) I. W. Hamley, *The Physics of Block Copolymers,* Oxford University Press, London, 1998.
(3) T. Okano, *Biorelated Polymers and Gels: Controlled Release and Applications in Biomedical Engineering,* Academic Press, San Diego, 1998.
(4) Y. Mogi, H. Kotsuji, Y. Kaneko, K. Mori, Y. Matsushita, and I. Noda, *Macromolecules,* **25**, 5408 (1992).
(5) Y. Mogi, M. Nomura, H. Kotsuji, K. Ohnishi, Y. Matsushita, and I. Noda, *Macromolecules,* **27**, 6755 (1994).
(6) C. Auschra and R. Stadler, *Macromolecules,* **26**, 2171 (1993).
(7) R. Stadler, C. Auschra, J. Beckmann, U. Krappe, I. Vight-Martin, and L. Leibler, *Macromolecules,* **28**, 3080 (1995).
(8) U. Krappe, R. Stadler, and I. Voigt-Martin, *Macromolecules,* **28**, 4558 (1995).
(9) U. Breiner, U. Krappe, and R. Stadler, *Macromol. Rapid Commun.,* **17**, 567 (1996).
(10) U. Breiner, U. Krapper, V. Abetz, and R. Stadler, *Macromol. Chem. Phys.,* **198**, 1051 (1997)
(11) V. Abetz and R. Stadler, *Macromol. Symp.,* **113**, 19 (1997).
(12) P. Alexandridis, J. F. Holzwarth, and T. A. Hatton, *Macromolecules,* **27**, 2414 (1994).
(13) M. Nguyen-Misra and W. L. Mattice, *Macromolecules,* **28**, 1444 (1995).
(14) Y.-W. Yang, Z. Yang, Z.-K. Zhou, D. Attwood, and C. Booth, *Macromolecules,* **29**, 670 (1996).
(15) Z. Zhou, B. Chu, V. M. Nace, Y.-W. Yang, and C. Booth, *Macromolecules,* **29**, 3663 (1996).
(16) J. R. Quintana, M. D. Janez, and I. Katime, *Langmuir,* **13**, 2640 (1997).
(17) S. L. Nolan, R. J. Phillips, P. M. Cotts, and S. R. Dungan, *J. Colloid & Inter. Sci.,* **191**, 291 (1997).
(18) J. R. Quintana, E. Diaz, and I. Katime, *Langmuir,* **14**, 1586 (1998).
(19) T. Liu, Z. Zhou, C. Wu, V. M. Nace, and B. Chu, *J. Phys. Chem. B,* **102**, 2875 (1998).
(20) C. Booth and D. Attwood, *Macromol. Rapid Commun.,* **21**, 501 (2000).
(21) M. J. Ko, S. H. Kim, and W. H. Jo, *Macromol. Theory Simul.,* **10**, 381 (2001).
(22) M. J. Ko, S. H. Kim, and W. H. Jo, *Macromolecules,* accepted for publication.
(23) M. J. Ko, S. H. Kim, and W. H. Jo, *Macromol. Theory Simul.,* submitted for publication.
(24) S. H. Kim and W. H. Jo, *Macromolecules,* in press.
(25) S. H. Kim and W. H. Jo, *Macromolecules,* submitted for publication.
(26) R. G. Larson, *Macromolecules,* **27**, 4198 (1994).
(27) X. Pan and J. S. Shaffer, *Macromolecules,* **29**, 4453 (1996).
(28) T. Pakula, K. Karatasos, S. H. Anastasiadis, and G. Fytas, *Macromolecules,* **30**, 8364 (1997).
(29) A. Hoffmann, J.-U. Sommer, and A. Blumen, *J. Chem. Phys.,* **107**, 7559 (1997).
(30) K. Kremer and G. S. Grest, *J. Chem. Phys.,* **92**, 5057 (1990).
(31) M. Murat, G. S. Grest, and K. Kremer, *Macromolecules,* **32**, 595 (1999).
(32) K. Binder, *Monte Carlo and Molecular Dynamics Simulations in Polymer Science,* Oxford University Press, New York, 1995.
(33) M. W. Matsen, *J. Chem. Phys.,* **108**, 785 (1998).
(34) S. Phan and G. H. Fredrickson, *Macromolecules,* **31**, 59 (1998).
(35) P. H. Nelson, G. C. Rutledge, and T. A. Hatton, *J. Chem. Phys.,* **107**,10777 (1997).
(36) D. Viduna, A. Milchev, and K. Binder, *Macromol. Theory Simul.,* **7**, 649 (1998).
(37) A. Milchev, A. Bhattacharya, and K. Binder, *Macromolecules,* **34**, 1881 (2001).
(38) M. D. Allen and D. J. Tildesley, in *Computer Simulation of Liquids,* Clarendon, Oxford, 1989.
(39) D. Frenkel and B. Smit, in *Understanding Molecu-*

lar Simulation, Academic Press, New York, 1996.
(40) C. M. Care and T. Dalby, *Europhys. Lett.,* **45**, 38 (1999).
(41) D. Attwood and A. T. Florence, in *Surfactant Systems: Their Chemistry, Pharmacy and Biology,* Chapman and Hall, London, 1983.
(42) F. K. von Gottberg, K. A. Smith, and T. A. Hatton, *J. Chem. Phys.,* **106**, 9850 (1997).
(43) M. A. Floriano, E. Caponetti, and A. Z. Panagiotopoulos, *Langmuir,* **15**, 3143 (1999).
(44) A. M. Ferrenberg and R. H. Swendsen, *Phys. Rev. Lett.,* **61**, 2635 (1988).
(45) A. M. Ferrenberg and R. H. Swendsen, *Phys. Rev. Lett.,* **63**, 1195 (1989).